Cyclophilin A is an inflammatory mediator that promotes atherosclerosis in apolipoprotein E–deficient mice

Patrizia Nigro,[1] Kimio Satoh,[1,3] Michael R. O'Dell,[1] Nwe Nwe Soe,[1] Zhaoqiang Cui,[1] Amy Mohan,[1] Jun-ichi Abe,[1] Jeffrey D. Alexis,[1] Janet D. Sparks,[2] and Bradford C. Berk[1]

[1]Aab Cardiovascular Research Institute, Department of Medicine and [2]Department of Pathology and Laboratory Medicine, University of Rochester School of Medicine and Dentistry, Rochester, NY 14642
[3]Department of Cardiovascular Medicine, Tohoku University Graduate School of Medicine, Aoba-ku, Sendai 980-8574, Japan

Cyclophilin A (CyPA; encoded by *Ppia*) is a ubiquitously expressed protein secreted in response to inflammatory stimuli. CyPA stimulates vascular smooth muscle cell migration and proliferation, endothelial cell adhesion molecule expression, and inflammatory cell chemotaxis. Given these activities, we hypothesized that CyPA would promote atherosclerosis. Apolipoprotein E–deficient ($Apoe^{-/-}$) mice fed a high-cholesterol diet for 16 wk developed more severe atherosclerosis compared with $Apoe^{-/-}Ppia^{-/-}$ mice. Moreover, CyPA deficiency was associated with decreased low-density lipoprotein uptake, VCAM-1 (vascular cell adhesion molecule 1) expression, apoptosis, and increased eNOS (endothelial nitric oxide synthase) expression. To understand the vascular role of CyPA in atherosclerosis development, bone marrow (BM) cell transplantation was performed. Atherosclerosis was greater in $Apoe^{-/-}$ mice compared with $Apoe^{-/-}Ppia^{-/-}$ mice after reconstitution with $CyPA^{+/+}$ BM cells, indicating that vascular-derived CyPA plays a crucial role in the progression of atherosclerosis. These data define a role for CyPA in atherosclerosis and suggest CyPA as a target for cardiovascular therapies.

CORRESPONDENCE
Bradford C. Berk:
bradford_berk@urmc.rochester.edu

Abbreviations used: BAEC, bovine aortic EC; CHX, cycloheximide; CsA, cyclosporine A; CyPA, cyclophilin A; DCF, dichlorofluorescein; DHE, dihydroethidium; EC, endothelial cell; eNOS, endothelial NO synthase; HUVEC, human umbilical vein EC; LDL, low-density lipoprotein; mRNA, messenger RNA; NO, nitric oxide; PI, propidium iodide; ROS, reactive oxygen species; siRNA, small interfering RNA; TUNEL, terminal deoxynucleotidyl transferase dUTP nick end labeling; VSMC, vascular smooth muscle cell.

Atherosclerosis is a disease of the vasculature that is characterized by chronic inflammation of the arterial wall (Hansson and Libby, 2006). The development of atherosclerosis is initiated by the activation of endothelial cells (ECs) leading to expression of adhesion molecules for inflammatory cells (Berk, 2008). In addition, these activated ECs facilitate the passage of lipid components in the plasma, such as low-density lipoproteins (LDLs; Hansson, 2005). A critical element in the progression of atherosclerosis is the development of an oxidizing environment caused by the activation of macrophages that become loaded with oxidized LDL and other lipids. These macrophages produce reactive oxygen species (ROS) and secrete cytokines and growth factors that contribute to the progression of atherosclerotic plaques and promote vulnerable lesions (Weber et al., 2008).

Cyclophilin A (CyPA) is a ubiquitously distributed protein belonging to the immunophilin family recognized as the intracellular receptor for the potent immunosuppressive drug cyclosporine A (CsA; Handschumacher et al., 1984). CyPA possesses peptidyl-prolyl isomerase activity and plays an important role in protein folding and trafficking (e.g., nuclear translocation of ERK1/2 [Pan et al., 2008] and AIF [apoptosis-inducing factor; Zhu et al., 2007]). Interestingly, it has been shown that CyPA is a part of a cytosolic trafficking complex consisting of caveolin, heat-shock protein 56, cyclophilin 40, CyPA, and cholesterol (Uittenbogaard et al., 1998). Although CyPA was initially believed to function primarily as an intracellular protein, recent studies have revealed that it can be secreted by cells in

P. Nigro and K. Satoh contributed equally to this paper.

The Rockefeller University Press $30.00
J. Exp. Med. Vol. 208 No. 1 53-66
www.jem.org/cgi/doi/10.1084/jem.20101174

The Journal of Experimental Medicine

response to inflammatory stimuli, especially ROS (Jin et al., 2000; Suzuki et al., 2006; Satoh et al., 2009). Extracellular CyPA is a potent leukocyte chemoattractant for human monocytes, neutrophils, eosinophils, and T cells (Sherry et al., 1992; Xu et al., 1992; Allain et al., 2002; Yurchenko et al., 2002; Arora et al., 2005; Damsker et al., 2007; Pan et al., 2008), and it stimulates inflammatory responses when injected in vivo (Sherry et al., 1992). Most importantly, plasma CyPA is significantly increased in patients with inflammatory diseases such as rheumatoid arthritis (Kim et al., 2005) and sepsis (Tegeder et al., 1997). We have shown that ROS promote secretion of CyPA from vascular smooth muscle cells (VSMCs; Jin et al., 2000; Liao et al., 2000) and that extracellular CyPA stimulates EC adhesion molecule expression in vitro (Jin et al., 2004; Suzuki et al., 2006). Furthermore, we found that CyPA mediates vascular remodeling by promoting inflammation and VSMC proliferation (Satoh et al., 2008), and it is indispensable for the development of angiotensin II–induced aortic aneurysms (Satoh et al., 2009; Weintraub, 2009).

Given these functions of CyPA, we hypothesized that CyPA would contribute to the development of atherosclerosis. In this study, we report that CyPA is atherogenic by enhancing LDL uptake, adhesion molecule expression, and inflammatory cell migration. Our data suggest that CyPA and its signaling pathways are novel targets for atherosclerosis therapy.

RESULTS

Atherosclerosis development is dependent on CyPA

To study the functional role of CyPA in atherogenesis, we used the *Apoe*$^{-/-}$ mouse, a well-known model of atherosclerosis (Nakashima et al., 1994). We generated *Apoe*$^{-/-}$*Ppia*$^{-/-}$ (double knockout) mice, and fed them a high-cholesterol diet for 16 wk. To visualize lipid-rich atherosclerotic plaques, aortas were stained with Oil red O. As shown in Fig. 1 A, *Apoe*$^{-/-}$*Ppia*$^{-/-}$ mice compared with *Apoe*$^{-/-}$ mice exhibited significantly less atherosclerosis: aortic coverage of 7.5 ± 2% in *Apoe*$^{-/-}$*Ppia*$^{-/-}$ versus 19.3 ± 8.2% in *Apoe*$^{-/-}$ (Fig. 1 B).

In another cohort of mice, we quantified plaque area in hematoxylin- and eosin (H&E)-stained cross sections of the aortic arch and thoracic aorta. Lesion area was significantly decreased in both the aortic arch (Fig. 1, C and D) and thoracic aorta (Fig. 1, C and E) of *Apoe*$^{-/-}$*Ppia*$^{-/-}$ mice compared with *Apoe*$^{-/-}$ mice. As expected, the elastic lamina was frequently degraded with large regions exhibiting disruption in *Apoe*$^{-/-}$ mice compared with *Apoe*$^{-/-}$*Ppia*$^{-/-}$ mice (Fig. S1). These results demonstrate a remarkable reduction in atherosclerosis in CyPA-deficient mice and strongly support our hypothesis that CyPA contributes to atherosclerosis.

The absence of CyPA decreases the lesion area and the migration of macrophages in the aortic sinus

The aortic sinus is particularly prone to intimal lesion development, and the cusps of the valves provide a useful positional cue in comparative experiments of sectioned tissues (Tangirala et al., 1995). As shown in Fig. 2 (A and B), *Apoe*$^{-/-}$*Ppia*$^{-/-}$ mice compared with *Apoe*$^{-/-}$ mice exhibited significantly less atherosclerosis measured by plaque area (H&E staining). There was also significantly less lipid deposition and cholesterol clefts in *Apoe*$^{-/-}$*Ppia*$^{-/-}$ mice (Fig. 2 A, Masson and Trichrome and Oil red O). Both H&E and Masson and Trichrome showed a significant reduction in intima formation in *Apoe*$^{-/-}$*Ppia*$^{-/-}$ mice (Fig. 2 A).

A crucial step in atherogenesis is the infiltration of monocytes into the subendothelial space of large arteries where they differentiate

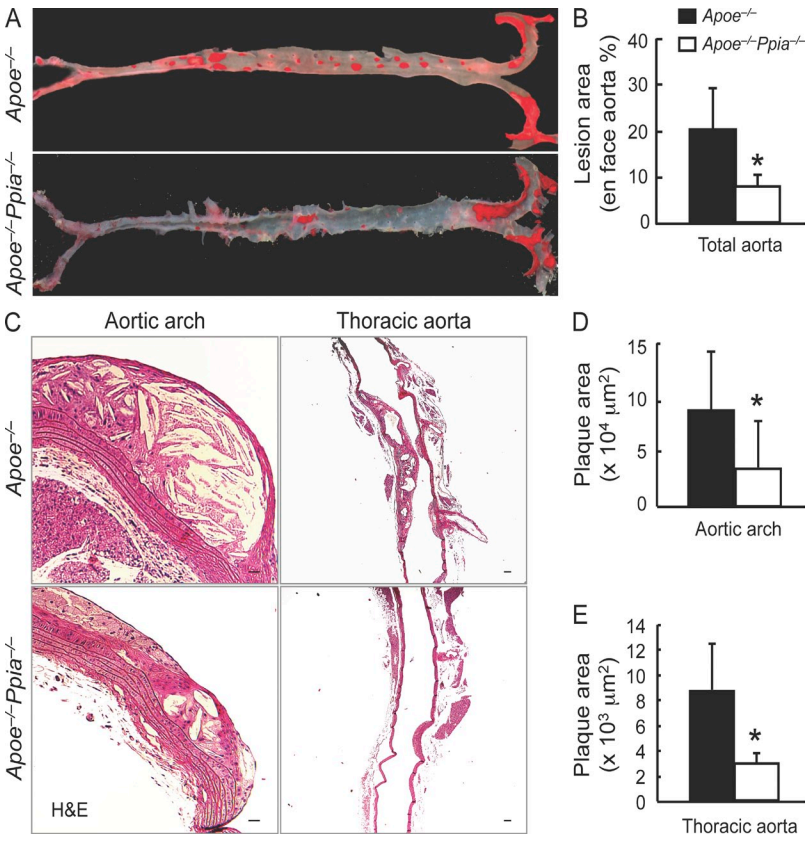

Figure 1. CyPA deficiency limits atherosclerosis formation. (A) Representative photographs showing Oil red O staining of aortas from *Apoe*$^{-/-}$ and *Apoe*$^{-/-}$*Ppia*$^{-/-}$ mice fed a high-cholesterol diet for 16 wk. (B) Lesion area was significantly decreased in *Apoe*$^{-/-}$*Ppia*$^{-/-}$ mice (n = 15) compared with *Apoe*$^{-/-}$ mice (n = 21). (C) Longitudinal cross sections from the aortic arch and thoracic aorta stained with H&E. Bars: (left) 25 µm; (right) 200 µm. (D and E) Quantification of plaque area showed that *Apoe*$^{-/-}$*Ppia*$^{-/-}$ mice (n = 7) exhibited decreased atherosclerosis compared with *Apoe*$^{-/-}$ mice (n = 9) in both the aortic arch (D) and thoracic aorta (E). (B, D, and E) Results are mean ± SD; *, P < 0.01 compared with *Apoe*$^{-/-}$ mice. Results in A–E show pooled data from two experiments.

into macrophages and become functionally active (Galkina and Ley, 2009). As shown in Fig. 2 (A and D), the *Apoe*$^{-/-}$*Ppia*$^{-/-}$ mice fed high-cholesterol diet for 16 wk showed significantly fewer Mac3-positive macrophages compared with the *Apoe*$^{-/-}$ mice. All these data suggest that CyPA is a key protein involved in the atherosclerosis progression and migration of inflammatory cells in the lesion area.

CyPA regulates LDL infiltration and the expression of scavenger receptors

Because it is well established that the transport of LDL cholesterol into the artery wall is the initiating event that triggers atherosclerosis (Glass and Witztum, 2001), we examined the role of CyPA in this process. To measure LDL uptake into vessels of *Apoe*$^{-/-}$ and *Apoe*$^{-/-}$*Ppia*$^{-/-}$ mice, we performed ex vivo incubation with fluorescent DiI-labeled LDLs and en face imaging of the aorta from the EC surface to a depth of 50 µm into the intima. CyPA deficiency caused a 43% decrease in DiI-LDL uptake in the lesser curvature of the aortic arch (atherosclerosis-prone area; Fig. 3, A and B; and Fig. S2). To strengthen this important finding, we confirmed these data with an independent method. *Apoe*$^{-/-}$ and *Apoe*$^{-/-}$*Ppia*$^{-/-}$ aortas were incubated with [^{125}I]LDL for a subsequent determination of incorporated radioactivity as measured by a gamma counter. As shown in Fig. S3, LDL uptake was significantly reduced in aortas from *Apoe*$^{-/-}$*Ppia*$^{-/-}$compared with *Apoe*$^{-/-}$ mice. To gain insight into how CyPA regulates lipid uptake, we examined expression of several scavenger receptors in aortas after 12 wk of high-cholesterol diet. The expression of lectin-like oxidized LDL receptor (LOX-1) and CD36 were significantly decreased in *Apoe*$^{-/-}$*Ppia*$^{-/-}$ mice compared with *Apoe*$^{-/-}$ mice, whereas SR-BI was decreased by an equivalent 40% (Fig. 3, C and D). The expression of SR-A did not differ significantly between *Apoe*$^{-/-}$ and *Apoe*$^{-/-}$*Ppia*$^{-/-}$ mice (Fig. 3, C and D). Collectively, the data demonstrate that CyPA influences LDL uptake by regulating the expression of scavenger receptors on the vessel wall.

CyPA deficiency induces the development of a more proatherogenic lipoprotein profile in *Apoe*$^{-/-}$ mice

Next, we performed phenotypic characterization of *Apoe*$^{-/-}$ and *Apoe*$^{-/-}$*Ppia*$^{-/-}$ mice fed a high-cholesterol diet for 16 wk. Body weights were similar in all the groups of mice before and after a high-cholesterol diet (Fig. S4 A). There were no significant differences in plasma cholesterol and triglyceride levels (Fig. S4, B and C). We next examined lipoprotein profiles by gel filtration chromatography (Fig. S4 D).

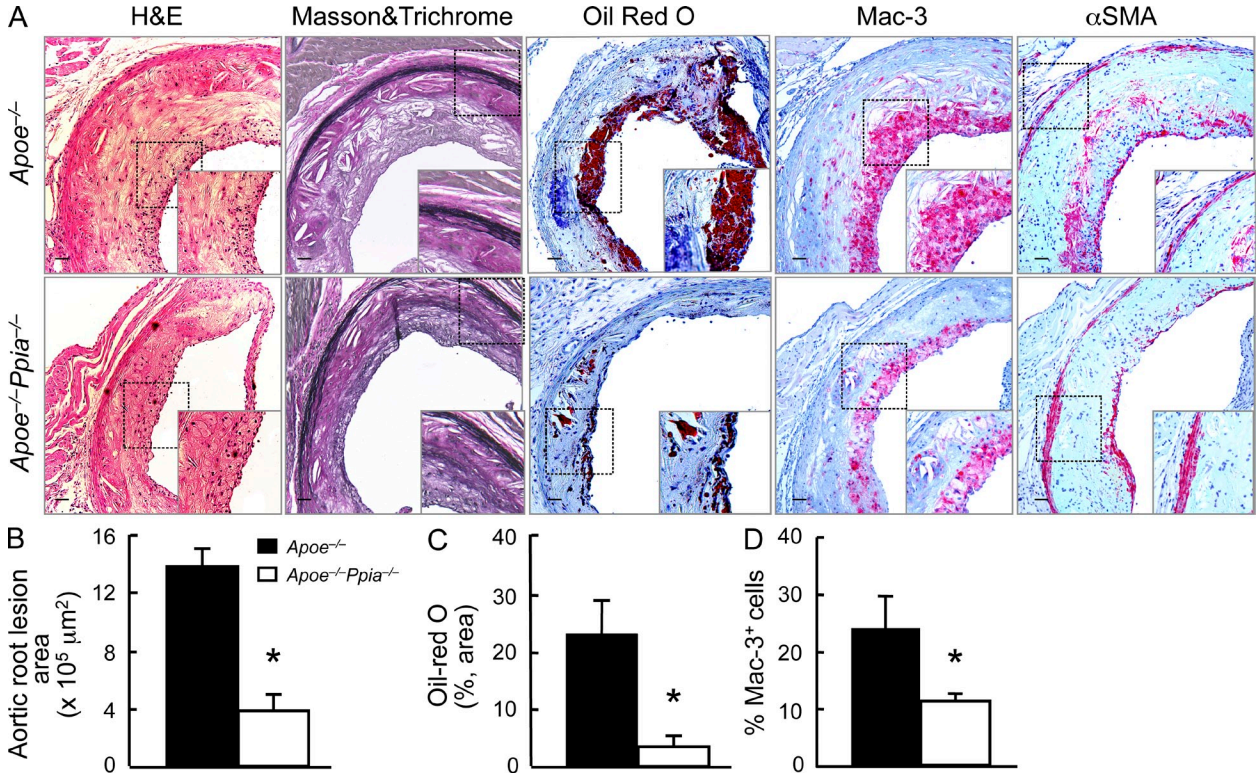

Figure 2. CyPA deficiency reduces lesion size and inflammatory cell accumulation in the aortic sinus. (A) Representative histological analysis of the aortic sinus stained with H&E, Masson and Trichrome, Oil red O, Mac3 (a macrophage marker), and α-smooth muscle cell actin (α-SMA). Insets are higher magnification images of the areas in the dashed boxes. Bars, 100 µm. (B–D) Quantification of the plaque area (B), lipid accumulation (C), and macrophage accumulation (D) shows a significant reduction in *Apoe*$^{-/-}$*Ppia*$^{-/-}$ mice (n = 7) compared with *Apoe*$^{-/-}$ (n = 9) mice. Results are mean ± SD; *, P < 0.01 compared with *Apoe*$^{-/-}$ mice. Results in A–D show pooled data from two experiments.

Although there were no differences observed in cholesterol and triglyceride levels, *Apoe*$^{-/-}$*Ppia*$^{-/-}$ mice demonstrated increases in the VLDL (very low-density lipoprotein)- and IDL (intermediate-density lipoprotein)/LDL-sized lipoproteins compared with *Apoe*$^{-/-}$ mice. No differences were observed in the HDL (high-density lipoprotein) fraction or in the levels of plasma apoB-100 and apoB-48 (Fig. S4 E). Collectively, these results indicate that loss of CyPA, in the context of the *Apoe*$^{-/-}$ genetic background, leads to the appearance of a more proatherogenic lipoprotein profile.

BM-derived CyPA does not play a significant role in atherosclerosis formation

CyPA has important roles in the immune system and is a well-described regulator of T lymphocyte functions (Colgan et al., 2004). Extracellular CyPA is a potent chemoattractant for inflammatory cells (Xu et al., 1992; Allain et al., 2002; Yurchenko et al., 2002). CyPA has also been reported to stimulate migration of BM-derived cells in vitro (Khromykh et al., 2007). To determine the role of BM-derived CyPA in atherosclerosis, BM transplantation experiments were performed.

BM cells from *Apoe*$^{-/-}$ and *Apoe*$^{-/-}$*Ppia*$^{-/-}$ mice were transplanted into 6-wk-old lethally irradiated *Apoe*$^{-/-}$ mice. After 4 wk of reconstitution, mice were fed with a high-cholesterol diet for 12 wk. Surprisingly, there were no differences in atherosclerosis measured by lesion area in the entire aorta (Fig. 4, A and B; Oil red O) or aortic root (Fig. 4, C and D; H&E). These data demonstrate that atherosclerosis in *Apoe*$^{-/-}$*Ppia*$^{-/-}$ mice was not altered by specific CyPA deficiency in BM-derived cells. Note that the atherosclerosis lesion area was reduced by ~50% in *Apoe*$^{-/-}$ mice after irradiation (compare Fig. 4 B with Fig. 1 B).

We next assessed the development of high-cholesterol–induced atherosclerosis in *Apoe*$^{-/-}$*Ppia*$^{-/-}$ chimeric mice that were transplanted with *Apoe*$^{-/-}$ BM or *Apoe*$^{-/-}$*Ppia*$^{-/-}$ BM. There was no significant difference in atherosclerosis lesions between the chimeric mice with *Apoe*$^{-/-}$ BM versus *Apoe*$^{-/-}$*Ppia*$^{-/-}$ BM (unpublished data).

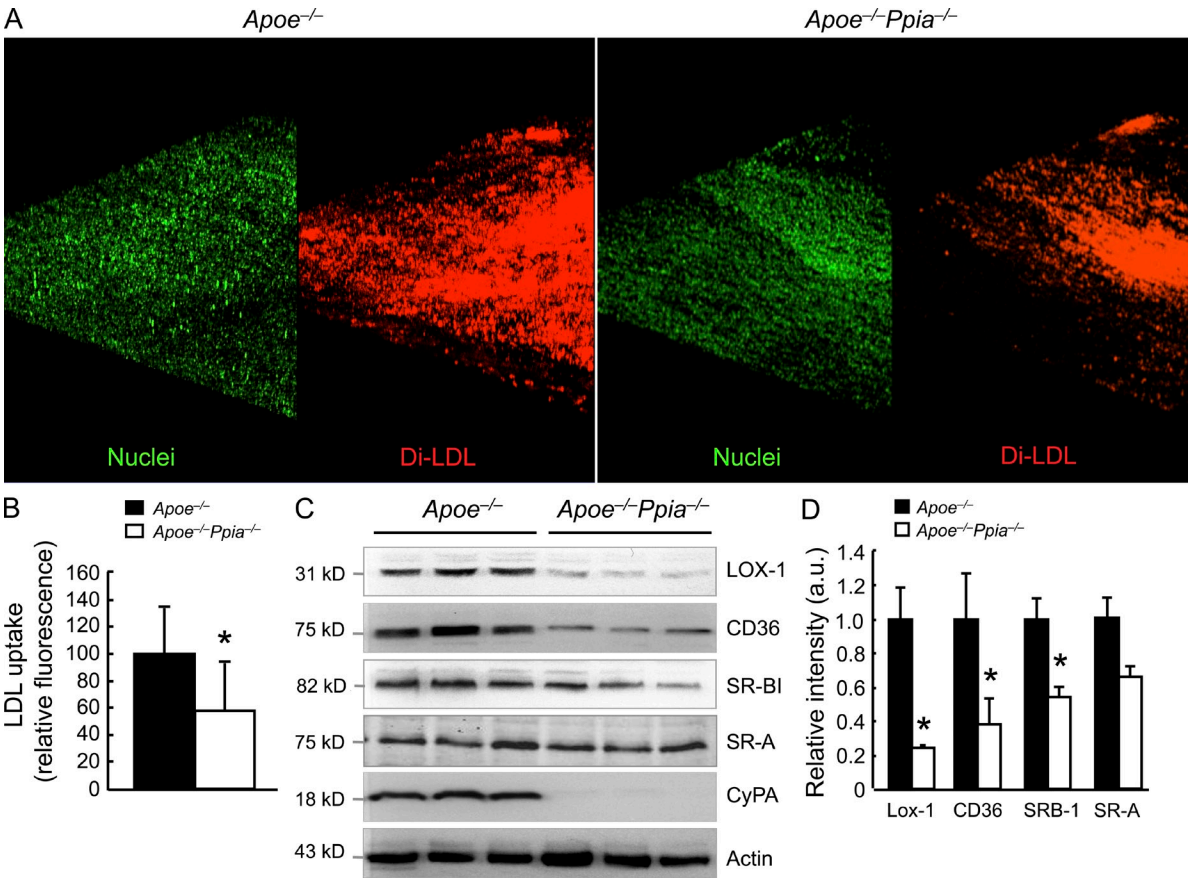

Figure 3. CyPA regulates LDL entry into the aortic wall and the expression of the scavenger receptors. (A) En face fluorescence images of aortic arches from 6-wk-old *Apoe*$^{-/-}$ and *Apoe*$^{-/-}$*Ppia*$^{-/-}$ mice (n = 3 each group) after incubation with DiI–labeled LDL (red) and SYTOX green nucleic acid stain (green). (B) Quantification of DiI-LDL fluorescence intensity from the en face images. The data are quantified as fluorescence-positive area. (C) Western blot analyses of aortic extracts from *Apoe*$^{-/-}$ and *Apoe*$^{-/-}$*Ppia*$^{-/-}$ mice fed a high-cholesterol diet for 12 wk. Results for three representative mice are shown for each genotype. (D) Densitometric analyses of the blots in C show significant decreases in LOX-1, CD36, and SR-BI scavenger receptors in *Apoe*$^{-/-}$*Ppia*$^{-/-}$ mice versus *Apoe*$^{-/-}$ mice. (B and D) Results are mean ± SD; *, $P < 0.01$ compared with *Apoe*$^{-/-}$ mice. Results in A–D show pooled data from two experiments.

To investigate the chemoattractive function of CyPA in vivo, we studied the trafficking of BM-derived cells into atherosclerotic lesions. To analyze BM cells that migrated into lesions, we used donor BM cells harvested from mice constitutively expressing the GFP protein (GFP$^+$ BM which are *Ppia*$^{+/+}$) and performed BM transplantation in lethally irradiated *Apoe*$^{-/-}$ and *Apoe*$^{-/-}$*Ppia*$^{-/-}$ mice. There was no significant difference in the reconstitution ratio (percentage of GFP$^+$ cells in the peripheral blood) in GFP$^+$ BM-transplanted *Apoe*$^{-/-}$*Ppia*$^{-/-}$ mice compared with GFP$^+$ BM-transplanted *Apoe*$^{-/-}$ mice. However, there was still a significant difference in the atherosclerosis lesion area in the *Apoe*$^{-/-}$ GFP$^+$ BM mice compared with *Apoe*$^{-/-}$*Ppia*$^{-/-}$ GFP$^+$ BM mice (9.6 ± 1.3% vs. 2.3 ± 0.3%), and migration of GFP$^+$ BM cells into the lesser curvature region was much greater in the *Apoe*$^{-/-}$ recipient mice (Fig. 4 E, left) compared with *Apoe*$^{-/-}$*Ppia*$^{-/-}$ recipient mice (Fig. 4 E, right) after high-cholesterol diet. High-magnification images (Fig. 4 G, top) showed the presence of enlarged foam cells in the *Apoe*$^{-/-}$ mice with GFP$^+$ BM (arrows), which is consistent with the concept that BM-derived cells differentiate into foam cells upon exposure to hyperlipidemia. Direct demonstration that the BM-derived GFP$^+$ cells were localized beneath the ECs (and not just adherent to the luminal surface) was obtained by examination of cross-sectional images of z-series stacks (Fig. 4 G, bottom). These results suggested that CyPA present in BM-derived cells is less important for recruitment to the sites of atherosclerosis lesions than CyPA present in vessels and other non-BM cells.

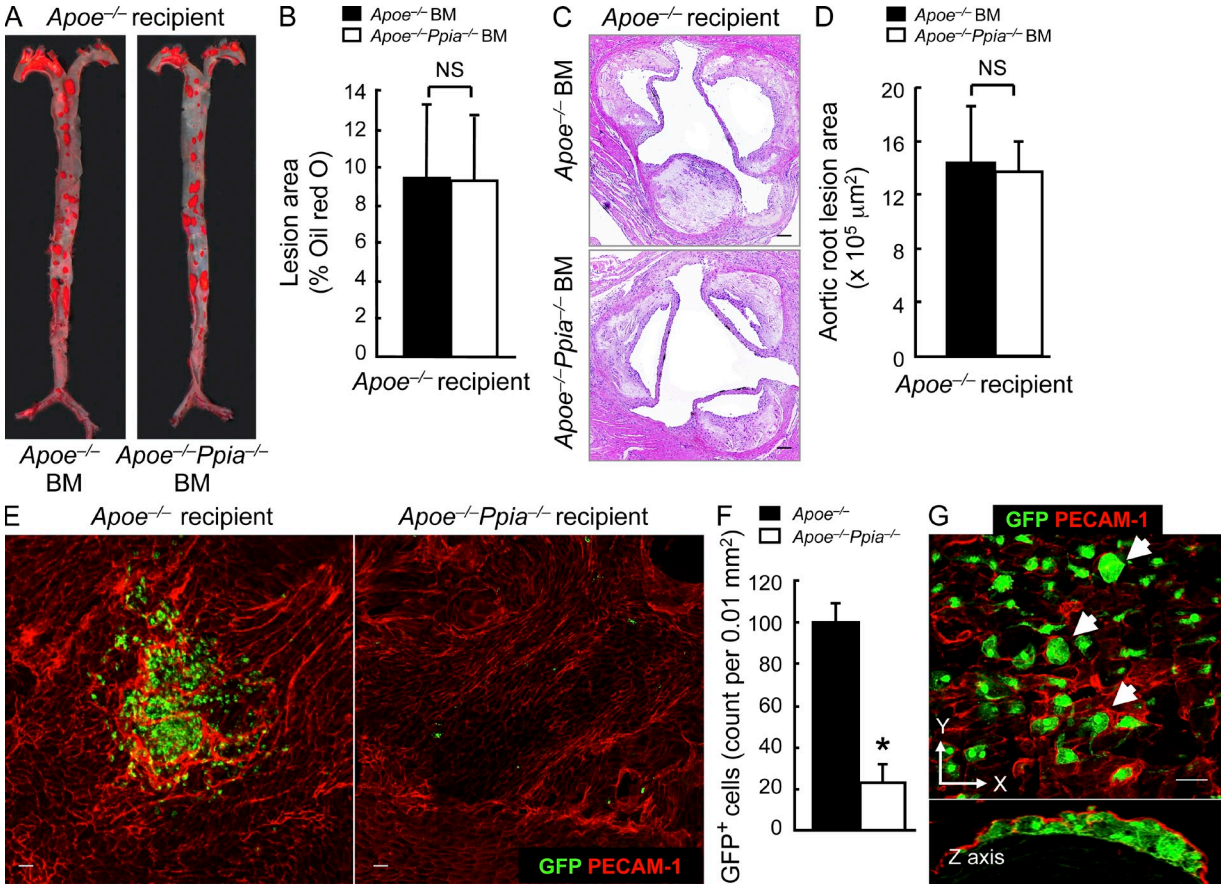

Figure 4. BM-derived CyPA is not crucial in atherosclerosis. (A) Representative Oil red O staining of aortas from *Apoe*$^{-/-}$ mice transplanted with *Apoe*$^{-/-}$ BM (n = 7) or *Apoe*$^{-/-}$*Ppia*$^{-/-}$ BM (n = 8) and fed a high-cholesterol diet for 12 wk. (B) Quantification of the lesion area shows that BM transplant of *Apoe*$^{-/-}$*Ppia*$^{-/-}$ cells does not decrease lesion development in *Apoe*$^{-/-}$ mice. (C and D) Representative histological analysis of aortic sinus stained with H&E (C) and quantification of the aortic root lesion area (D). (B and D) Results are mean ± SD; P > 0.01. (E) *Ppia*$^{+/+}$ BM cells (GFP$^+$) were transplanted into irradiated *Apoe*$^{-/-}$ (n = 4) or *Apoe*$^{-/-}$*Ppia*$^{-/-}$ (n = 4) mice as described in Materials and methods. Representative PECAM-1 en face staining (Alexa Fluor 546; red) and migration of the GFP$^+$ cells in aortic arch from *Apoe*$^{-/-}$ and *Apoe*$^{-/-}$*Ppia*$^{-/-}$ mice with *Ppia*$^{+/+}$ BM under high-cholesterol diet for 12 wk. (F) Number of migrating GFP$^+$ cells was dramatically higher in the aortic wall of *Apoe*$^{-/-}$ (n = 4) compared with *Apoe*$^{-/-}$*Ppia*$^{-/-}$ mice (n = 4). Results are mean ± SD; *, P < 0.01 compared with *Apoe*$^{-/-}$ mice. (G) En face confocal microscopy of aortic arch from *Apoe*$^{-/-}$ mice transplanted with GFP$^+$ cells. Top panel shows foam cells, which were identified by large size and diffuse GFP pattern (arrows). Bottom panel shows the reconstruction in z axis of the images shown in the top panel. GFP$^+$ cells are clearly present in the subendothelial space defined by the PECAM-1 positive fluorescence above them. Results in A–G show pooled data from two experiments. Bars: (C) 100 µm; (E and G) 10 µm.

CyPA regulates endothelial nitric oxide (NO) synthase (eNOS) expression

The aforementioned results suggest that the athero protection observed in the *Apoe*$^{-/-}$*Ppia*$^{-/-}$ was caused by decreased inflammation mediated by the absence of CyPA. The vascular endothelium by virtue of its strategic location between the plasma and the underlying tissue is endowed with a large array of functions that are vital for the initiation of atherosclerosis. Therefore, we performed an extensive examination of the endothelium of aortic arch and thoracic aorta by using PECAM-1 en face staining to visualize ECs. *Apoe*$^{-/-}$*Ppia*$^{-/-}$ mice showed a decreased EC disorganization in both the aortic segments when compared with *Apoe*$^{-/-}$ mice (Fig. S5, A and B).

To evaluate further the mechanisms by which CyPA promotes inflammation, we measured VCAM-1 (vascular cell adhesion molecule 1) expression, which is highly expressed in activated ECs and promotes atherosclerosis (Cybulsky and Gimbrone, 1991; Nakashima et al., 1998; Cybulsky et al., 2001). En face staining (Fig. 5, A and B) of aortic tissues showed that VCAM-1 expression was significantly reduced in mice lacking CyPA.

eNOS function is critical for vascular homeostasis via generation of NO, and its loss is proatherogenic (Knowles et al., 2000; Chen et al., 2001; Kuhlencordt et al., 2001; Kawashima and Yokoyama, 2004). Furthermore, the progression of atherosclerosis is associated with decreases in both eNOS expression (Oemar et al., 1998; Handa et al., 2008) and NO production (Li and Förstermann, 2009). Therefore, we compared eNOS expression in aortas from *Apoe*$^{-/-}$ and *Apoe*$^{-/-}$*Ppia*$^{-/-}$ mice by en face staining. As shown in Fig. 6 A, eNOS protein expression was significantly higher in the *Apoe*$^{-/-}$*Ppia*$^{-/-}$ mice compared with *Apoe*$^{-/-}$ mice. In addition, the location of eNOS differed, being predominantly perinuclear in the *Apoe*$^{-/-}$ mice and diffuse (especially membrane associated) in the *Apoe*$^{-/-}$*Ppia*$^{-/-}$ mice. To define the mechanisms responsible for decreased eNOS expression, we studied the effect of altering CyPA levels in cultured human umbilical vein ECs (HUVECs). To increase eNOS expression and stimulate cellular responses that are atheroprotective, cells were placed in a cone and plate viscometer, and steady laminar s-flow at physiological shear stress (12 dyn/cm^2; termed s-flow here) was applied. As shown in Fig. 6 (B and C), s-flow–mediated induction of eNOS was significantly increased by

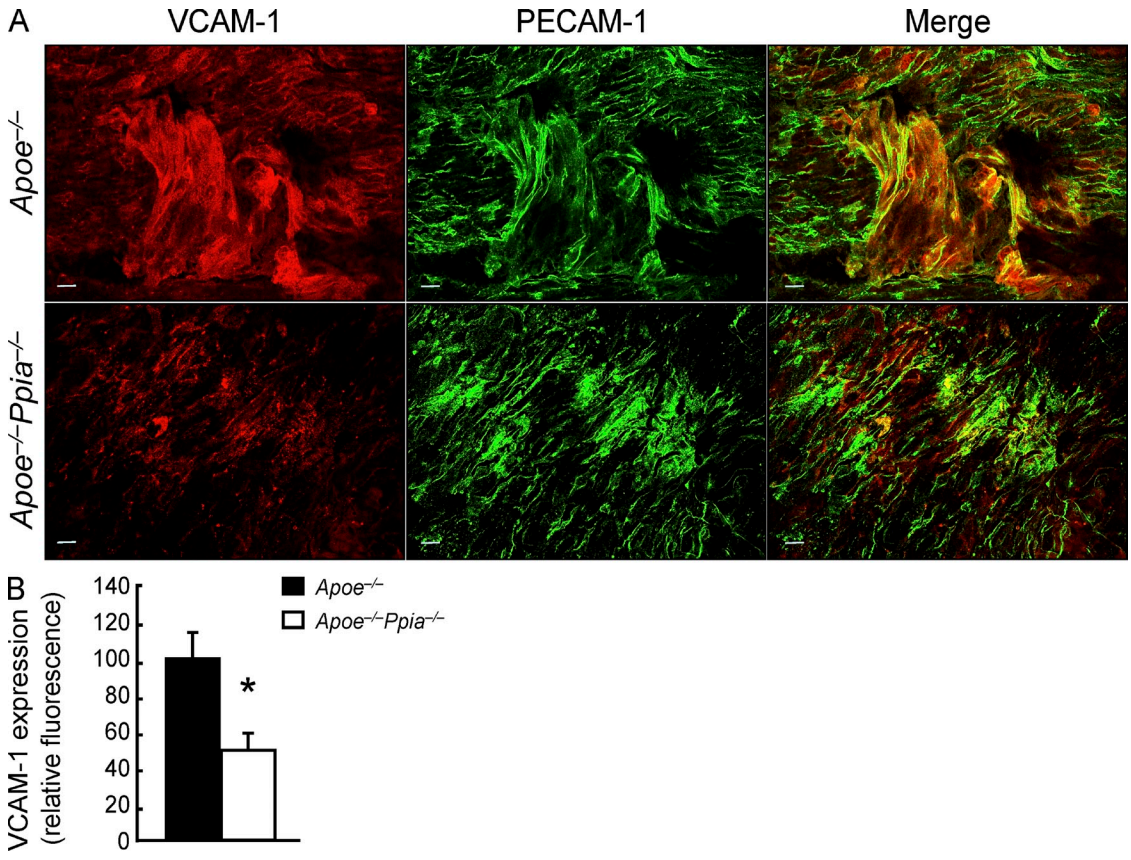

Figure 5. VCAM-1 expression is significantly down-regulated in *Apoe*$^{-/-}$*Ppia*$^{-/-}$ mice compared with *Apoe*$^{-/-}$ mice. (A) Representative en face staining for VCAM-1 expression (Alexa Fluor 546; red) in the aortic arch. EC morphology was changed in the atherosclerosis regions where ECs are stretched and may have lost PECAM-1 staining (Alexa Fluor 488; green) at some cell junctions. Bars, 10 µm. (B) Densitometric analysis of the en face staining also shows a significant reduction in VCAM-1 expression in *Apoe*$^{-/-}$*Ppia*$^{-/-}$ mice compared with *Apoe*$^{-/-}$ mice ($n = 4$ each group). Results are mean ± SD; *, $P < 0.01$ compared with *Apoe*$^{-/-}$ mice. Results in A and B show pooled data from two experiments.

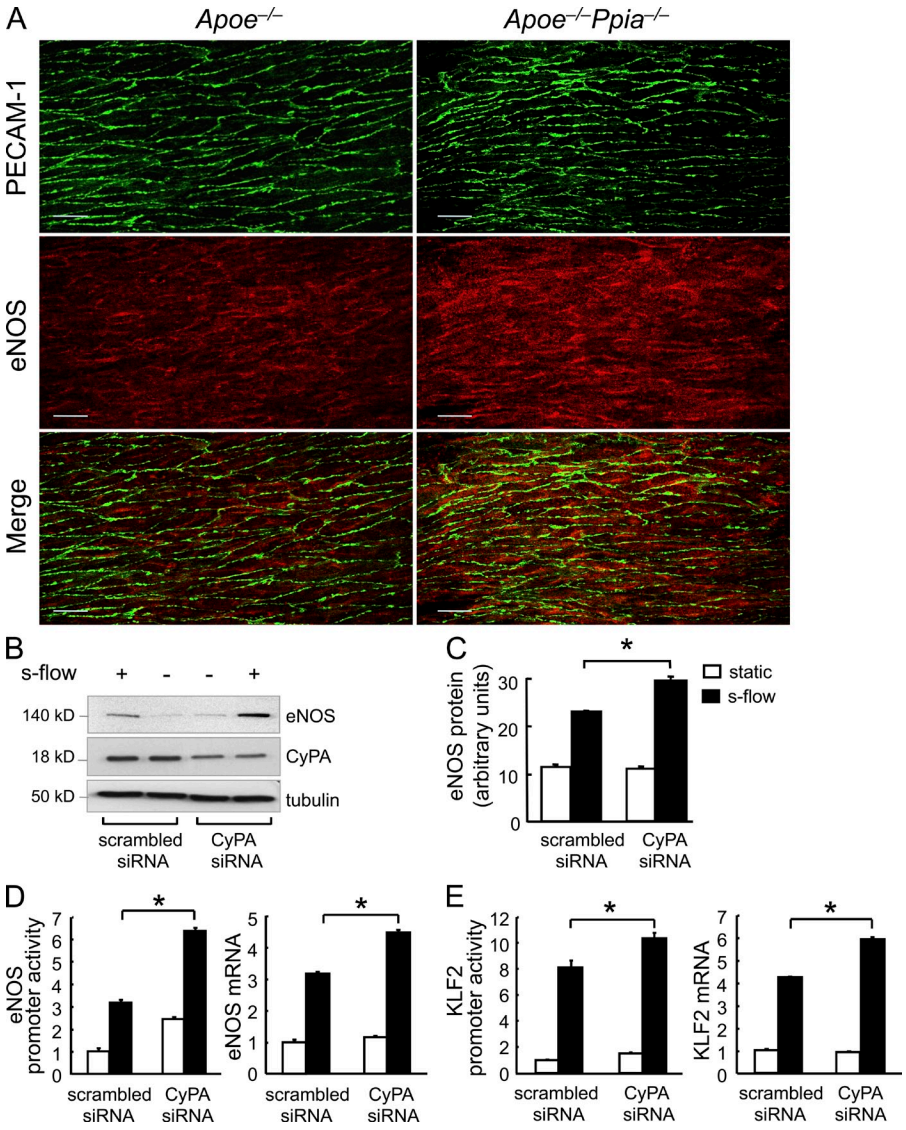

Figure 6. CyPA deficiency and s-flow are associated with increased eNOS expression. (A) Aortas from 12-wk *Apoe*$^{-/-}$ and *Apoe*$^{-/-}$*Ppia*$^{-/-}$ mice were harvested for qualitative analysis of eNOS expression (Alexa Fluor 546; red) by en face dual staining immunofluorescence. PECAM-1 staining (Alexa Fluor 488; green) was used to identify the EC layer. Note that these images were obtained from the thoracic aorta, a region of s-flow. eNOS protein expression was higher in *Apoe*$^{-/-}$*Ppia*$^{-/-}$ mice compared with *Apoe*$^{-/-}$ mice aortas (relative fluorescence of 147 ± 18.48 in *Apoe*$^{-/-}$*Ppia*$^{-/-}$ vs. 100 ± 13.61 in *Apoe*$^{-/-}$; $n = 3$ each group). Bars, 10 µm. (B and C) HUVECs were transfected with CyPA siRNA or scrambled siRNA for 48 h as described in Materials and methods and then exposed to s-flow for 24 h. Western blot analysis shows significantly greater eNOS expression after depletion of CyPA. (D and E) HUVECs were treated for 48 h with CyPA siRNA or scrambled siRNA and then transfected with eNOS (D) or KLF2 (E) promoter. Cells were then exposed to s-flow or maintained in static condition. To evaluate the promoter function, luciferase activity was measured after 24 h. To measure eNOS and KLF2 mRNA levels, a quantitative PCR analysis was performed. (C–E) Results are mean ± SD of three independent experiments performed in triplicate. *, $P < 0.01$ versus scrambled siRNA.

CyPA small interfering RNA (siRNA). Also, CyPA knockdown in HUVECs increased eNOS promoter activity and eNOS messenger RNA (mRNA) levels (Fig. 6 D). Parmar et al. (2006) have shown that the s-flow induction of the KLF2 (Kruppel-like factor 2) transcription factor stimulates eNOS mRNA expression through the ERK5–MEF2–KLF2 pathway. Therefore, we examined whether CyPA could regulate KLF2 expression. As expected, s-flow increased KLF2 promoter activity and KLF2 mRNA levels (Fig. 6 E). These effects were significantly increased by CyPA knockdown. To further substantiate the role of CyPA in the regulation of eNOS expression, we transfected HUVECs with WT CyPA (CyPA-WT). Overexpression of CyPA was accompanied by down-regulation of eNOS at protein (Fig. 7, A and B) and mRNA levels (Fig. 7 C). Consistent with the expression data, overexpression of CyPA decreased eNOS promoter activity in HUVECs (Fig. 7 D). Finally, overexpression of CyPA decreased KLF2 promoter activity (Fig. 7 E) and mRNA levels in HUVECs (Fig. 7 F). These findings illustrate a novel mechanism by which CyPA promotes atherosclerosis, through suppression of KLF2 expression and consequent repression of eNOS transcription.

CyPA affects eNOS expression by a ROS-dependent mechanism

ROS are key mediators of signaling pathways that underlie vascular inflammation in atherogenesis. We have previously shown that CyPA is a key determinant for ROS generation, contributing to the onset of vascular inflammation during aortic aneurism formation (Satoh et al., 2009). Therefore, we evaluated whether ROS are downstream mediators of CyPA in the pathophysiologic context of inflammation we observed. We first overexpressed CyPA in ECs, and then we evaluated the basal level of ROS by dichlorofluorescein (DCF; Fig. 8 A) and dihydroethidium (DHE; Fig. 8 B) staining. ROS production was significantly higher in ECs overexpressing CyPA compared with cells transfected with the vector control (4.2- and 1.6-fold increase in DCF and DHE fluorescence, respectively). These data suggest that CyPA plays a critical role in ROS generation in ECs similar to our findings in VSMCs (Satoh et al., 2009).

To demonstrate that ROS are key determinants in CyPA-mediated inflammation, we evaluated whether CyPA decreases eNOS expression by a ROS-dependent mechanism. Both the antioxidants *N*-acetyl-cysteine and Tiron, by rebalancing excessive ROS production induced by CyPA overexpression, reversed the CyPA-mediated inhibition of eNOS (Fig. 8 C) and KLF2 promoter activity (Fig. 8 D). These data demonstrated that CyPA induces inflammation through ROS-dependent mechanisms. Based on these results, we believe that CyPA, acting as a proinflammatory cytokine, synergistically augments ROS production, contributing to vascular inflammation and atherogenesis.

Deletion of CyPA decreases EC apoptosis

To ascertain whether intracellular CyPA may participate in the EC apoptosis, we knocked down CyPA in bovine aortic ECs (BAECs) by siRNA and measured hypodiploidia (sub-G_1 cell count) after treatment with TNF plus cycloheximide (CHX) as apoptogens. TNF promoted 11.95 ± 0.07% cell death in cells transfected with scrambled siRNA, and this effect was significantly decreased to 6.65 ± 0.07% by using CyPA siRNA (Fig. 9 A). To better discriminate between apoptosis and necrosis (sub-G_1 cell count might also include necrotic cells), we performed the double staining with annexin V (FITC) and propidium iodide (PI), followed by flow cytometry analysis. Representative cytograms in Fig. 9 B show that cells transfected with scrambled siRNA and treated with TNF plus CHX increased both the percentage of cells gated in the top right quadrant (annexin$^+$/PI$^+$; late apoptotic/necrotic cells) and in the bottom right quadrant (annexin$^+$/PI$^-$; early apoptosis). Transfection of CyPA siRNA significantly attenuated this effect. Moreover, ECs lacking CyPA showed less cleaved caspase-3 expression by Western blot analysis (Fig. 9 C). Because EC apoptosis has been suggested as an initial step in atherogenesis, we studied EC apoptosis in the early stages of the lesion development in mice fed with a high-cholesterol diet for only 1 mo. As shown in Fig. 9 (D and E), there was a marked decrease in apoptotic ECs (detected by terminal deoxynucleotidyl transferase dUTP nick end labeling [TUNEL] staining) in aortic lesions from *Apoe*$^{-/-}$*Ppia*$^{-/-}$ mice compared with littermate control mice. These data underline the crucial role of CyPA during the apoptotic process that is an important early event for the development of atherosclerosis.

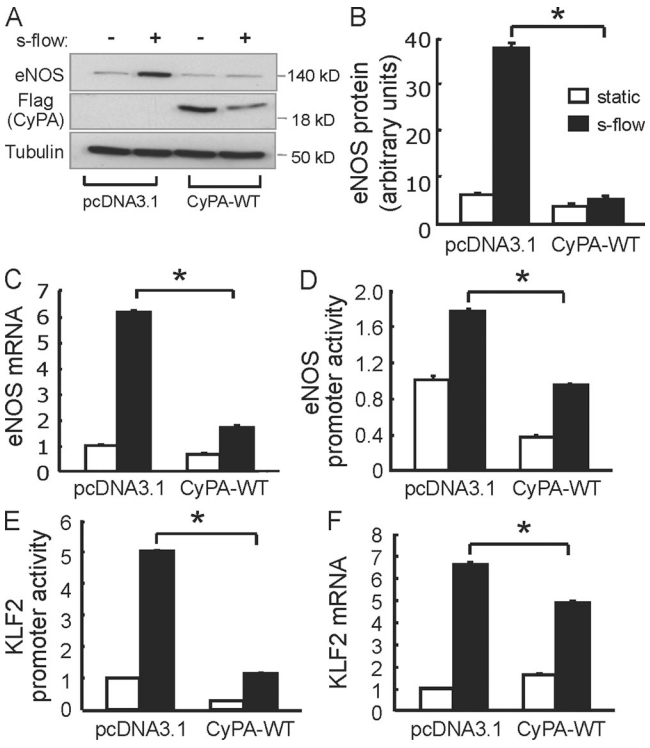

Figure 7. CyPA overexpression decreases eNOS and KLF2 expression. (A) HUVECs were transfected with CyPA-WT for 24 h and then exposed to static and s-flow condition for a further 24 h. (A–F) Western blot data and quantitative PCR analysis revealed that CyPA overexpression inhibited s-flow–induced eNOS protein (A and B), eNOS mRNA (C), and also KLF2 mRNA (F) levels. HUVECs were cotransfected with CyPA-WT and with either eNOS (D) or KLF2 (E) promoter. The cells were exposed to static or s-flow condition, and the luciferase activity was measured after 24 h. Overexpression of CyPA decreases eNOS and KLF2 promoter activity. Data are the mean values ± SD of three independent experiments performed in triplicate. *, $P < 0.01$ versus control pcDNA3.1.

DISCUSSION

The major finding of this study is that CyPA deficiency in vivo decreases atherosclerotic lesion burden in a mouse model of atherosclerosis. We characterized five important pathological mechanisms by which vascular CyPA promotes atherosclerosis. First, CyPA increases LDL uptake in the vessel wall by regulating the expression of scavenger receptors. Second, CyPA increases EC activation and inflammation by increasing VCAM-1 expression. Third, CyPA decreases eNOS expression through KLF2 transcriptional repression. Fourth, CyPA is a key determinant for TNF-induced EC apoptosis. Finally, CyPA stimulates recruitment of inflammatory cells derived from the BM to the aortic wall. All of these mechanisms, while promoting an environment of oxidative stress, are likely to contribute to the increased atherosclerosis observed in the *Apoe*$^{-/-}$*Ppia*$^{+/+}$ mice.

The decrease in Oil red O staining is consistent with the decrease of multiple lipid uptake receptors in vessels of *Apoe*$^{-/-}$*Ppia*$^{-/-}$ mice. It is likely that CyPA regulates scavenger receptor expression by multiple mechanisms. Because CyPA is a chaperone protein, it may be necessary for appropriate folding and/or transport of LOX-1 and CD36 to the cell membrane. CD36 is mainly expressed in caveolae, and CyPA is essential for caveolae formation via transport of cholesterol and caveolin-1 (Uittenbogaard et al., 1998; Everson and Smart, 2001). In addition, both LOX-1 and CD36 are highly regulated by ROS and cytokines, which are markedly reduced in the *Apoe*$^{-/-}$*Ppia*$^{-/-}$ mice.

The decrease in VCAM-1 expression and increase in eNOS expression observed in *Apoe*$^{-/-}$*Ppia*$^{-/-}$ mice likely contributes to less inflammation. The decrease in VCAM-1

may be causally related to increased eNOS expression because it was previously shown that eNOS can down-regulate VCAM-1 expression (Kawashima et al., 2001). Consequently, there will be reduced monocyte adhesion to the endothelium, transmigration into the subendothelial space, and inflammation. It may be relevant to note that VCAM-1 expression appears to precede lesion formation (Nakashima et al., 1998; Cybulsky et al., 2001), suggesting an important role for CyPA in the initiation of atherosclerotic lesions. Moreover, we found that CyPA decreased eNOS expression by repressing KLF2 at the transcriptional level. This finding is of significant interest because KLF2 is a central regulator of EC biology (Atkins and Jain, 2007), and it has recently been shown that hemizygous deficiency of KLF2 increased high-cholesterol diet–induced atherosclerosis in *Apoe*$^{-/-}$ mice (Atkins et al., 2008). KLF2 also protects ECs from oxidative stress–mediated injury and subsequent apoptosis (Parmar et al., 2006). The mechanism by which CyPA negatively regulated KLF2 function remains to be elucidated, although a nuclear function for CyPA has been suggested for CXCR4 signaling (Pan et al., 2008).

An essential role for CyPA in apoptosis has become increasingly apparent. We showed that extracellular CyPA promoted EC apoptosis in association with increased JNK (c-Jun N-terminal kinase) and p38 activities (Jin et al., 2004). In this study, we found that knockdown of CyPA in ECs reduced TNF-induced apoptosis in vitro, and CyPA deficiency was associated with a marked decrease in EC apoptosis in early stages of atherosclerosis. A likely mechanism for CyPA-mediated apoptosis is binding and nuclear translocation of AIF (Zhu et al., 2007). In addition, the increase in the vascular oxidative stress requires CyPA (Satoh et al., 2009) and thereby sensitizes ECs to apoptosis.

CyPA may play an important role in several stages of atherosclerosis. During fatty streak formation, it may play a role in lipid uptake via its effect on scavenger receptors. In all

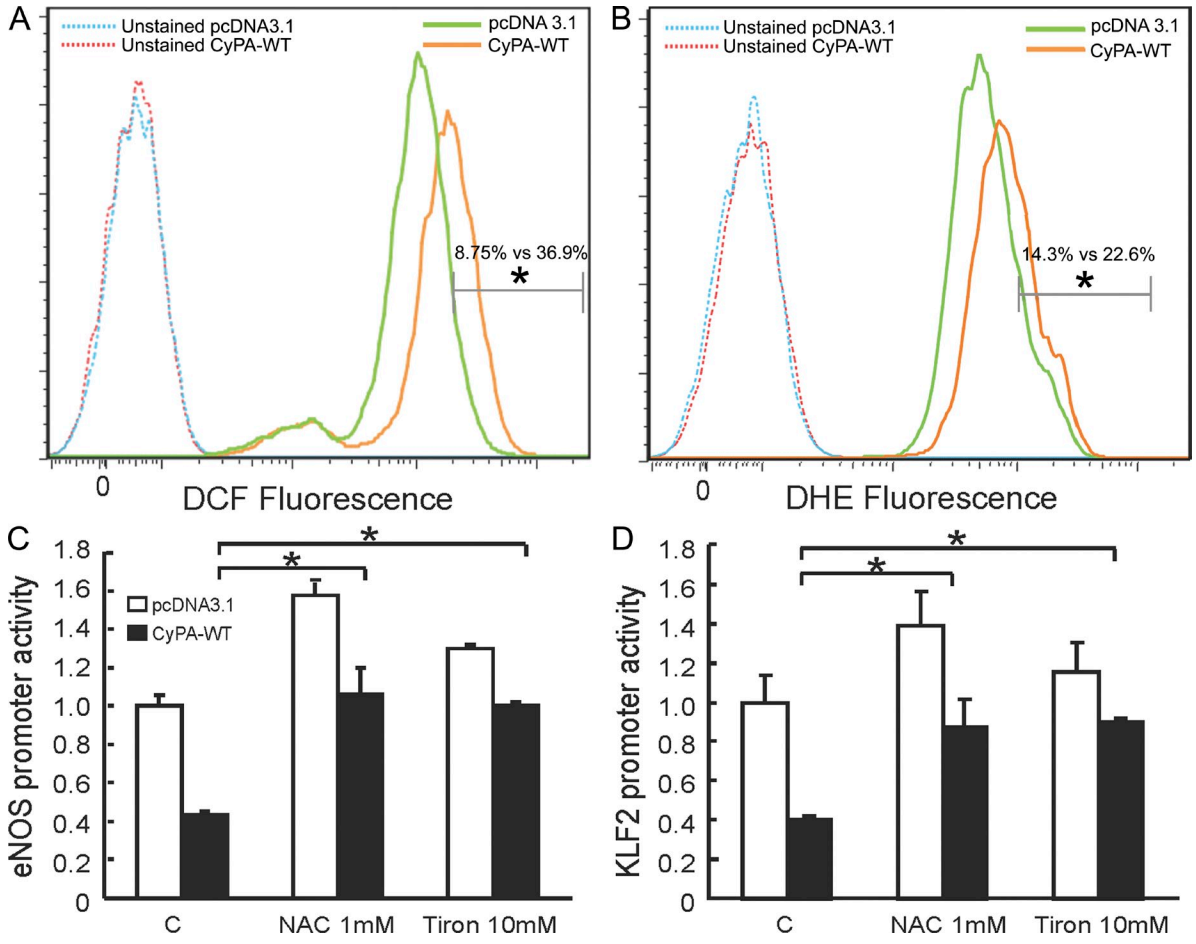

Figure 8. CyPA increases ROS levels in ECs. (A and B) HUVECs were transfected with CyPA-WT and vector control. After 48 h of incubation, ROS levels were measured by determining DCF (A) and DHE (B) fluorescence. CyPA overexpression significantly increased ROS content in cells. Data are the representation of three independent experiments performed in triplicate. *, $P < 0.01$ vs. control pcDNA3.1. (C and D) HUVECs were transfected with CyPA-WT and vector control. After 24 h, cells were treated with 1 mM *N*-acetyl-cysteine and 10 mM Tiron. 16 h later, eNOS (C) and KLF2 (D) promoter activity were measured by luciferase assay. Data are the mean values ± SD of three independent experiments performed in triplicate. *, $P < 0.01$ versus control pcDNA3.1.

stages, it may play a role in inflammation by promoting monocyte adhesion and recruitment as well as contributing to an oxidative environment. The data from Seizer et al. (2010) showing that CyPA is secreted from foam cells suggest an important role in later stages of atherosclerosis. Finally, we have recently shown an essential role for CyPA for matrix metalloproteinase activation (Satoh et al., 2009), suggesting that CyPA may also play an important role in plaque rupture. Altogether, our data suggest that the agents that inhibit CyPA expression or agents that block CyPA receptors might be candidates that may regulate atherosclerotic plaque and its rupture.

We would like to point out that studies in animals and humans, although contradictory and not conclusive, have reported that CsA, the immunosuppressive drug that inhibits CyPA, increases hyperlipidemia and risk of atherosclerosis (Fernández-Miranda et al., 1998; Ojo, 2006; Kockx et al., 2010). We also reported that decreasing cholesterol content in caveolae by CsA is a potentially important pathogenic mechanism for CsA-induced endothelial dysfunction and atherosclerosis (Lungu et al., 2004). These findings appear to contradict our data. However, the diversity of the pathways affected by CsA does not allow for simple conclusions to be drawn. CsA also affects many cellular pathways not associated

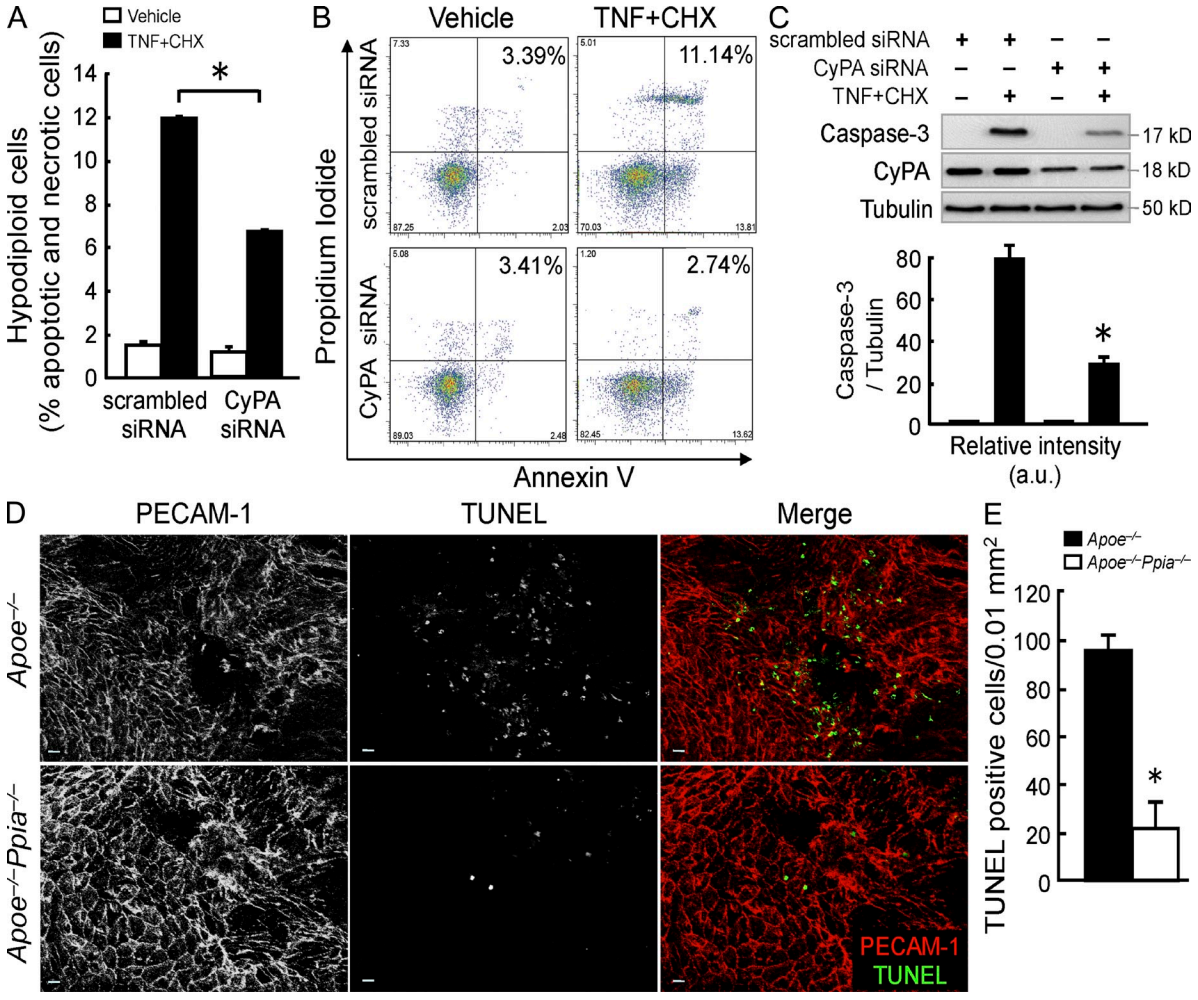

Figure 9. CyPA deficiency reduces EC apoptosis in vitro and in vivo. (A) BAECs were transfected with CyPA siRNA or scrambled siRNA for 48 h and then treated with 10 ng/ml TNF + 10 µg/ml CHX for 6 h. Apoptotic cells were determined by their hypochromic, subdiploid staining profiles (sub-G_1 population). The data represent the mean ± SD of triplicate samples repeated in three separate experiments. *, $P < 0.01$ versus scrambled siRNA. (B) Dot-plot diagrams of FITC-conjugated annexin V– and PI-stained cells after treatment with TNF + CHX for 3 h. Results are representative of two separate experiments that gave similar results. (C) Western blot analyses of cleaved caspase-3 in BAECs treated with TNF + CHX for 6 h. Data represent the mean ± SD of three separate experiments. *, $P < 0.01$ versus scrambled siRNA. (D) Whole-mount en face dual immunofluorescence staining of *Apoe*$^{-/-}$ and *Apoe*$^{-/-}$*Ppia*$^{-/-}$ mice aortas after 4 wk of a high-cholesterol diet. Note that these images were obtained from the inner curvature of the aortic arch, which is a region of disturbed flow. PECAM-1 staining shows polygonal ECs that are not aligned with flow. TUNEL staining shows increased fluorescence in *Apoe*$^{-/-}$ mice. Bars, 10 µm. (E) Quantitative data show that *Apoe*$^{-/-}$*Ppia*$^{-/-}$ mice aortas have a significant decrease in apoptotic cells in the lesion area. The data are expressed as the percentage of TUNEL-positive cells per field (four fields per three mice each group). *, $P < 0.01$ compared with *Apoe*$^{-/-}$ mice. Results are the mean ± SD and show pooled data from two experiments.

with immunosuppression, several of which can be linked to its cardiovascular side effects. Moreover, CsA is not a selective drug for CyPA. In fact, CyPA, -B, and -C all bind with high affinity to CsA in vitro (Bram et al., 1993). Therefore, the proatherogenic effect of CsA could be related to the inhibition of other cyclophilin isoforms. In addition, CsA could promote atherosclerosis by a CyPA-independent mechanism. For example, CsA directly binds to LDL and affects LDL metabolism at several levels (López-Miranda et al., 1993; Vaziri et al., 2000). We believe that the discovery of more uniquely selective and specific inhibitors of CyPA will be a good therapeutic approach for atherosclerosis.

MATERIALS AND METHODS

Animal procedures. All animal experiments were conducted in accordance with experimental protocols that were approved by the University Committee on Animal Resources at the University of Rochester. *Ppia*$^{-/-}$ mice were purchased from The Jackson Laboratory and were backcrossed to C57BL/6J mice for 10 generations. The *Apoe*$^{-/-}$ mice on a C57BL/6J background were obtained from The Jackson Laboratory. Double knockout *Apoe*$^{-/-}$*Ppia*$^{-/-}$ mice were generated by crossing *Ppia*$^{-/-}$ mice with *Apoe*$^{-/-}$ mice. The F1 generation was backcrossed with *Apoe*$^{-/-}$ mice to fix the *Apoe*$^{-/-}$ genotype, and littermates were crossed. All mice were genotyped by PCR on tail clip samples, and all experiments were performed with generations F4–F6 using littermate *Apoe*$^{-/-}$*Ppia*$^{+/+}$ as controls. Animals were housed under a 12-h light and 12-h dark regimen. Accelerated atherosclerosis was induced by feeding the mice for 16 wk with a high-cholesterol diet containing 1.25% cholesterol (Research Diets D12108C).

Atherosclerotic lesion analysis. Mice were anesthetized with an intraperitoneal injection of 80 mg kg^{-1} ketamine and 5 mg kg^{-1} xylazine. Hearts were perfused through the left ventricle with PBS followed by 10% buffered formaldehyde. After fixation overnight in 10% formaldehyde, the aortas were thoroughly cleaned under a dissecting microscope. All adventitial fat and connective tissue was carefully removed. The vessels were then cut open longitudinally through the inner curvature and the ventral portions of the thoracic and abdominal sections. Aortas were rinsed with 5 ml of 60% isopropanol for 5 min. Staining was performed with 5 ml of filtered Oil red O solution (Poly Scientific) for 15 min. Vessels were then rinsed with 60% isopropanol for 15 min, followed by a final rinse with distilled water. After staining, the greater curvature of the aorta was cut to divide the arch in half. The vessel was precisely pinned to black wax in PBS to reveal the entire luminal surface area. Images were obtained using SPOT version 4.1.1, a camera (SPOT Insight 4; Diagnostic Instruments, Inc.) connected to a microscope (MZ12.5; Leica). Plaques were analyzed in Photoshop 8.0 (Adobe), and lesion area was quantified using Image-Pro Analyzer 6.2 (Media Cybernetics).

Histological analysis. Mice were anesthetized and euthanized. For morphological analysis, aortas were perfused with normal saline and fixed with 10% phosphate-buffered formalin at physiological pressure for 5 min (Satoh et al., 2008). The whole aortas and hearts were harvested, fixed for 24 h, and embedded in paraffin, and 5-µm cross sections were prepared. Paraffin sections were stained with H&E or Masson and Trichrome or used for immunostaining. Analyses were performed by using Image-Pro Plus software (Media Cybernetics).

Immunohistochemistry. Formaldehyde-fixed paraffin sections were incubated with primary antibody overnight at 4°C. The primary antibodies used were Mac3 (clone M3/84; 1:200 dilution; BD) and α-smooth muscle actin (clone 1A4; 1:1,000 dilution; Sigma-Aldrich). As a negative control, species- and isotype-matched IgG were used in place of the primary antibody. Slides were viewed with a microscope (BX41; Olympus) and with digital camera (SPOT Insight 2; Diagnostic Instruments, Inc.). Vessel areas and densitometric analysis were measured with Image-Pro Plus software.

En face analysis. Immunofluorescence staining of mouse aortic ECs was performed as described previously (Won et al., 2007). Aortas were perfused with PBS followed by 2% paraformaldehyde for 10 min. After fixation, the aortas were cut in small segments and incubated in blocking buffer containing 2% BSA. Primary antibody incubations were performed overnight at 4°C. The primary antibodies used were VCAM-1 (1:200; Santa Cruz Biotechnology, Inc.), eNOS (1:100; BD), and PECAM-1 (1:200; BD). After washing the aortic segments three times, secondary antibodies were added and incubated for 1 h. Negative controls included addition of nonimmune goat or rabbit IgG. After washing, aortic specimens were opened, placed on a glass slide with the luminal side up, and then mounted for confocal microscopy (FLUOVIEW; Olympus).

Ex vivo LDL tissue uptake. *Apoe*$^{-/-}$ and *Apoe*$^{-/-}$*Ppia*$^{-/-}$ mice were anesthetized and euthanized. Aortas were dissected, cut in small fragments, and incubated in 50 µg/ml DiI-LDL. After 2 h, aortas were washed with PBS and fixed using 4% paraformaldehyde. Then, aortic segments were opened and stained with SYTOX green nucleic acid stain (dilution 1:10,000; Invitrogen). After washing, the aortic specimens were prepared for en face analysis by confocal microscopy (FLUOVIEW). Analysis of different images was performed using Image-Pro Plus software. The results are expressed in terms of fluorescence-positive areas for each animal (n = 3 each group, 4 fields each animal). Human LDL was isolated by ultracentrifugation (1.019 g/ml < d < 1.063 g/ml) and dialyzed against 0.15 M NaCl/1 mM EDTA overnight at 4°C using a 50,000 MWCO dialysis membrane. The LDL (250 µg) was directly iodinated using iodobeads (Thermo Fisher Scientific) as described by the manufacturer, and unincorporated ^{125}I was removed by two rounds of gel filtration on PD10 columns (GE Healthcare) using PBS, pH 7.0, as elution buffer. The ^{125}I-labeled LDL was adjusted to a specific activity of 500 dpm/ng by addition of unlabeled LDL and then filter sterilized using 0.2 µm Acrodisk syringe filter (Pall Life Sciences). More than 98% of the radioactivity in the [^{125}I]LDL preparation was precipitable with trichloroacetic acid. For [^{125}I]LDL uptake experiments, aortas (n = 4 each group) were incubated with 10 µg/ml [^{125}I]LDL in serum-free medium. After a 3-h incubation at 37°C, aortas were washed three times with 2 ml PBS and assayed for cell-associated label and protein content (Podrez et al., 1999). Measurement of radioactivity was performed in a gamma counter (Wallac 1470 Automatic Gamma Counter; EG&G Wallac).

Western blot analysis. Aortic tissue samples were frozen with liquid nitrogen, crushed, and lysed in cell lysis buffer (Cell Signaling Technology) with protease inhibitor cocktail (Sigma-Aldrich). HUVECs and BAECs were washed twice with PBS and harvested on ice in radioimmunoprecipitation assay lysis buffer (50 mmol/l Hepes, 10 mmol/l EDTA, 150 mmol/l NaCl, 1% NP-40, 0.5% Na deoxycholate, and 0.1% SDS, pH 7.4) supplemented with the protease inhibitor cocktail. Total cell lysates were loaded on SDS-PAGE and electrotransferred into nitrocellulose membrane followed by blocking 1 h at room temperature in 5% nonfat dry milk in PBS/0.1% Tween 20. After being washed three times with PBS/0.1% Tween 20, the blots were incubated overnight at 4°C with the appropriate primary antibody. The primary antibodies used were CyPA (1:5,000 dilution; Enzo Life Sciences, Inc.), LOX-1 (1:1,000 dilution; Abcam), SR-BI (1:1,000 dilution; Abcam), CD36 (1:1,000 dilution; Santa Cruz Biotechnology, Inc.), VCAM-1 (1:2,000 dilution; Santa Cruz Biotechnology, Inc.), actin (1:5,000 dilution; Santa Cruz Biotechnology, Inc.), eNOS (1:1,000 dilution; BD), α-tubulin (1:5,000 dilution; Sigma-Aldrich), Flag (1:2,000 dilution; Sigma-Aldrich), and caspase-3 (1:1,000 dilution; Cell Signaling Technology). ApoB isoforms present in serum were determined by immunoblotting with rabbit anti–rat apoB antibodies prepared in our laboratory (Chirieac et al., 2000). The membranes were incubated with peroxidase-conjugated secondary antibodies for 1 h. Signals were visualized using the enhanced chemiluminescence Western blotting detection system (GE Healthcare). Images were acquired with a

Gel Doc system (Gel Doc 2000; Bio-Rad Laboratories), and a densitometric analysis of membranes was performed using the Bio-Rad Laboratories software.

Lipids analysis and lipoprotein profiles measurement. Mice were anesthetized, and blood samples were collected from the left ventricle. Plasma was prepared and stored at −80°C. Plasma cholesterol and triglycerides were enzymatically measured using the Cholesterol E kit (Wako Chemicals USA, Inc.) and Infinity Triglyceride kit (Thermo Fisher Scientific), respectively, according to the manufacturers' instructions. Lipoproteins in pooled plasma samples (100 µl) from nine $Apoe^{-/-}$ mice and nine $Apoe^{-/-}Ppia^{-/-}$ mice were assessed by fast performance liquid chromatography using a Superose 6 HR 10/30 column (GE Healthcare) at a flow rate of 0.4 ml/min. Cholesterol and triglyceride concentrations were measured in each fraction by the aforementioned methods.

BM transplantation. BM transplantation was performed as described previously (Satoh et al., 2006). In brief, recipient mice were lethally irradiated and received an intravenous injection of 5×10^6 donor BM cells suspended in 100 µl of calcium- and magnesium-free PBS with 2% FBS. After transplantation, the mice were placed on a regular chow diet for 6 wk followed by high-cholesterol diet for 12 wk. Transgenic mice ubiquitously expressing GFP were obtained from The Jackson Laboratory. The chimeric rate assessed by reconstitution with GFP^+ BM cells was >99% by FACS analysis (FACSCanto II; BD).

BM-derived cell recruitment assays. Quantitative numbers or percentages of the migrating GFP^+ cells was analyzed by en face staining as reported in En face analysis. PECAM-1 antibody was used to identify the EC by using a FLUOVIEW confocal microscope.

Cell culture and transfection. HUVECs were obtained from collagenase-digested umbilical veins and collected in M200 medium supplemented with low serum growth supplement (Invitrogen), 5% fetal calf serum (Invitrogen), 50 U/ml penicillin, and 50 µg/ml streptomycin. BAECs were cultured in M199 medium (Invitrogen) supplemented with 10% fetal clone III (Hyclone), MEM–amino acids, 50 U/ml penicillin, and 50 µg/ml streptomycin. HUVECs as well as BAECs were cultured on 2% gelatin–precoated dishes. For transient expression experiments, 80% confluent cells were transfected using Opti-MEM and Lipofectamine 2000 (Invitrogen). 3 h after transfection, Opti-MEM was replaced with complete media, and cells were exposed to flow 24 h later. For siRNA-driven depletion of CyPA, HUVECs and BAECs were transiently transfected with 100 nM scrambled siRNA or CyPA siRNA using Lipofectamine 2000 reagent. The cells were used 48 h after siRNA transfection.

Steady laminar flow (s-flow) protocol. Confluent cells cultured in 100-mm dishes were exposed to flow in a cone and plate viscometer placed in an incubator with 5% CO_2 at 37°C for 24 h (shear stress = 12 dyn/cm^2).

eNOS and KLF2 promoter activity. HUVECs were transiently cotransfected with human eNOS promoter (provided by D. Gardner, University of California, San Francisco, San Francisco, CA) or KLF2 promoter (provided by J. Lingrel, University of Cincinnati, Cincinnati, OH) and β-galactosidase using Lipofectamine 2000. After 8 h, the cells were exposed to flow. 24 h later, cells were lysed in passive lysis buffer (Promega). Luciferase assays were performed using the Luciferase assay system (Promega). Luciferase activity was normalized to β-galactosidase activity to correct for differences in transfection efficiency.

Real-time quantitative PCR analysis of eNOS and KLF2. Total RNA was isolated by TRIZOL reagent (Invitrogen), and reverse transcription was conducted by using TaqMan reverse transcription reagents (Applied Biosystems) according to the manufacturer's instructions. The relative quantities of mRNAs were obtained using the comparative Ct method and were normalized by GAPDH (Applied Biosystems).

ROS measurement. The evaluation of ROS production was performed as described previously (Griendling and FitzGerald, 2003). After transfection with CyPA-WT and vector control for 48 h, HUVECs were washed with PBS and loaded with 10 µM 2,7-DCF diacetate (H2DCF-DA; Invitrogen) or 5 µM DHE (Invitrogen) for 30 min at 37°C. ROS levels were measured using flow cytometry (FACSCanto II). Data from 20,000 events per sample were collected, and forward light scatter characteristics were evaluated to exclude cell debris from the analysis.

Apoptosis analysis. Apoptotic cells were determined by analyzing their subdiploid staining profiles (sub-G_1 population). BAECs were cultured in the presence of TNF + CHX and then washed in PBS, resuspended (5×10^5 cells/ml) in PI hypotonic solution (0.1% Na citrate, 0.1% Triton X-100, and 50 µg/ml PI), and left at 4°C for 30 min in the dark. Data from 20,000 events per sample were collected by flow cytometry (FACSCanto II). Forward light scatter characteristics were used so that cell debris could be excluded from the analysis. For the estimation of apoptotic cells, cells were collected and double labeled with FITC-conjugated annexin V and PI according to the manufacturer's instructions (Trevigen). Green (FITC-conjugated annexin V) and red (PI) fluorescence of individual cells were measured by flow cytometry (FACSCanto II). Electronic compensation was required to exclude overlapping of the two emission spectra. For the detection of apoptosis on the whole aortic mount, FITC-labeled dUTP nick end labeling (TUNEL) method was applied to the aortic segments by using an In Situ Apoptosis Detection kit-POD according to the manufacturer's instruction (Roche). Images were acquired by confocal microscopy (FLUOVIEW).

Statistical analyses. Quantitative results are expressed as mean ± SD. Comparisons of parameters among two groups were made by the unpaired Student's *t* test. Comparisons of parameters among the three groups were made by one-way analysis of variance, and comparisons of different parameters between the two genotypes were made by two-way analysis of variance, followed by a post hoc analysis using the Bonferroni test. Statistical significance was evaluated with StatView (StatView 5.0; SAS Institute, Inc.). A value of $P < 0.05$ was considered to be statistically significant.

Online supplemental material. Fig. S1 shows that CyPA deficiency prevents atherosclerosis formation. Fig. S2 shows that CyPA deficiency decreases LDL uptake in the lesser curvature of the mouse aorta. Fig. S3 shows that CyPA regulates LDL uptake. Fig. S4 shows metabolic parameters in the absence of CyPA. Fig. S5 shows that CyPA promotes EC damage and disorganization. Online supplemental material is available at http://www.jem.org/cgi/content/full/jem.20101174/DC1.

We are grateful to the Aab Cardiovascular Research Institute members for useful suggestions and Mary A. Georger, Joanne Cianci, and Chelsea Wong for technical assistance. We are also grateful to Eiichiro Yamamoto for assisting with data analysis.

This work was supported by National Institutes of Health grant HL49192 (to B.C. Berk), Internal Grant of the University of Salerno (to P. Nigro), Japan Heart Foundation/Bayer Yakuhin Research Grant Abroad (to K. Satoh), Japan Heart Foundation/Novartis Grant for Research Award on Molecular and Cellular Cardiology (to K. Satoh), AstraZeneca Research Grant (to K. Satoh), and grants-in-aid from the Japanese Ministry of Education, Culture, Sports, Science and Technology (to K. Satoh).

The authors declare no competing financial interests.

Submitted: 11 June 2010
Accepted: 23 November 2010

REFERENCES

Allain, F., C. Vanpouille, M. Carpentier, M.C. Slomianny, S. Durieux, and G. Spik. 2002. Interaction with glycosaminoglycans is required for cyclophilin B to trigger integrin-mediated adhesion of peripheral blood T lymphocytes to extracellular matrix. *Proc. Natl. Acad. Sci. USA*. 99:2714–2719. doi:10.1073/pnas.052284899

Arora, K., W.M. Gwinn, M.A. Bower, A. Watson, I. Okwumabua, H.R. MacDonald, M.I. Bukrinsky, and S.L. Constant. 2005. Extracellular cyclophilins contribute to the regulation of inflammatory responses. *J. Immunol*. 175:517–522.

Atkins, G.B., and M.K. Jain. 2007. Role of Krüppel-like transcription factors in endothelial biology. *Circ. Res.* 100:1686–1695. doi:10.1161/01.RES.0000267856.00713.0a

Atkins, G.B., Y. Wang, G.H. Mahabeleshwar, H. Shi, H. Gao, D. Kawanami, V. Natesan, Z. Lin, D.I. Simon, and M.K. Jain. 2008. Hemizygous deficiency of Krüppel-like factor 2 augments experimental atherosclerosis. *Circ. Res.* 103:690–693. doi:10.1161/CIRCRESAHA.108.184663

Berk, B.C. 2008. Atheroprotective signaling mechanisms activated by steady laminar flow in endothelial cells. *Circulation.* 117:1082–1089. doi:10.1161/CIRCULATIONAHA.107.720730

Bram, R.J., D.T. Hung, P.K. Martin, S.L. Schreiber, and G.R. Crabtree. 1993. Identification of the immunophilins capable of mediating inhibition of signal transduction by cyclosporin A and FK506: roles of calcineurin binding and cellular location. *Mol. Cell. Biol.* 13: 4760–4769.

Chen, J., P.J. Kuhlencordt, J. Astern, R. Gyurko, and P.L. Huang. 2001. Hypertension does not account for the accelerated atherosclerosis and development of aneurysms in male apolipoprotein e/endothelial nitric oxide synthase double knockout mice. *Circulation.* 104:2391–2394. doi:10.1161/hc4501.099729

Chirieac, D.V., L.R. Chirieac, J.P. Corsetti, J. Cianci, C.E. Sparks, and J.D. Sparks. 2000. Glucose-stimulated insulin secretion suppresses hepatic triglyceride-rich lipoprotein and apoB production. *Am. J. Physiol. Endocrinol. Metab.* 279:E1003–E1011.

Colgan, J., M. Asmal, M. Neagu, B. Yu, J. Schneidkraut, Y. Lee, E. Sokolskaja, A. Andreotti, and J. Luban. 2004. Cyclophilin A regulates TCR signal strength in CD4+ T cells via a proline-directed conformational switch in Itk. *Immunity.* 21:189–201. doi:10.1016/j.immuni.2004.07.005

Cybulsky, M.I., and M.A. Gimbrone Jr. 1991. Endothelial expression of a mononuclear leukocyte adhesion molecule during atherogenesis. *Science.* 251:788–791. doi:10.1126/science.1990440

Cybulsky, M.I., K. Iiyama, H. Li, S. Zhu, M. Chen, M. Iiyama, V. Davis, J.C. Gutierrez-Ramos, P.W. Connelly, and D.S. Milstone. 2001. A major role for VCAM-1, but not ICAM-1, in early atherosclerosis. *J. Clin. Invest.* 107:1255–1262. doi:10.1172/JCI11871

Damsker, J.M., M.I. Bukrinsky, and S.L. Constant. 2007. Preferential chemotaxis of activated human CD4+ T cells by extracellular cyclophilin A. *J. Leukoc. Biol.* 82:613–618. doi:10.1189/jlb.0506317

Everson, W.V., and E.J. Smart. 2001. Influence of caveolin, cholesterol, and lipoproteins on nitric oxide synthase: implications for vascular disease. *Trends Cardiovasc. Med.* 11:246–250. doi:10.1016/S1050-1738(01)00119-0

Fernández-Miranda, C., C. Guijarro, A. de la Calle, C. Loinaz, I. Gonzalez-Pinto, T. Gómez-Izquierdo, S. Larumbe, E. Moreno, and A. del Palacio. 1998. Lipid abnormalities in stable liver transplant recipients—effects of cyclosporin, tacrolimus, and steroids. *Transpl. Int.* 11:137–142. doi:10.1111/j.1432-2277.1998.tb00789.x

Galkina, E., and K. Ley. 2009. Immune and inflammatory mechanisms of atherosclerosis (*). *Annu. Rev. Immunol.* 27:165–197. doi:10.1146/annurev.immunol.021908.132620

Glass, C.K., and J.L. Witztum. 2001. Atherosclerosis. The road ahead. *Cell.* 104:503–516. doi:10.1016/S0092-8674(01)00238-0

Griendling, K.K., and G.A. FitzGerald. 2003. Oxidative stress and cardiovascular injury: Part I: basic mechanisms and in vivo monitoring of ROS. *Circulation.* 108:1912–1916. doi:10.1161/01.CIR.0000093660.86242.BB

Handa, S., A.M. Sadi, M.I. Cybulsky, D.J. Stewart, and M. Husain. 2008. Region-specific patterns of vascular remodelling occur early in atherosclerosis and without loss of smooth muscle cell markers. *Atherosclerosis.* 196:617–623. doi:10.1016/j.atherosclerosis.2007.06.032

Handschumacher, R.E., M.W. Harding, J. Rice, R.J. Drugge, and D.W. Speicher. 1984. Cyclophilin: a specific cytosolic binding protein for cyclosporin A. *Science.* 226:544–547. doi:10.1126/science.6238408

Hansson, G.K. 2005. Inflammation, atherosclerosis, and coronary artery disease. *N. Engl. J. Med.* 352:1685–1695. doi:10.1056/NEJMra043430

Hansson, G.K., and P. Libby. 2006. The immune response in atherosclerosis: a double-edged sword. *Nat. Rev. Immunol.* 6:508–519. doi:10.1038/nri1882

Jin, Z.G., M.G. Melaragno, D.F. Liao, C. Yan, J. Haendeler, Y.A. Suh, J.D. Lambeth, and B.C. Berk. 2000. Cyclophilin A is a secreted growth factor induced by oxidative stress. *Circ. Res.* 87:789–796.

Jin, Z.G., A.O. Lungu, L. Xie, M. Wang, C. Wong, and B.C. Berk. 2004. Cyclophilin A is a proinflammatory cytokine that activates endothelial cells. *Arterioscler. Thromb. Vasc. Biol.* 24:1186–1191. doi:10.1161/01.ATV.0000130664.51010.28

Kawashima, S., and M. Yokoyama. 2004. Dysfunction of endothelial nitric oxide synthase and atherosclerosis. *Arterioscler. Thromb. Vasc. Biol.* 24:998–1005. doi:10.1161/01.ATV.0000125114.88079.96

Kawashima, S., T. Yamashita, M. Ozaki, Y. Ohashi, H. Azumi, N. Inoue, K. Hirata, Y. Hayashi, H. Itoh, and M. Yokoyama. 2001. Endothelial NO synthase overexpression inhibits lesion formation in mouse model of vascular remodeling. *Arterioscler. Thromb. Vasc. Biol.* 21:201–207.

Khromykh, L.M., N.L. Kulikova, T.V. Anfalova, T.A. Muranova, V.M. Abramov, A.M. Vasiliev, V.S. Khlebnikov, and D.B. Kazansky. 2007. Cyclophilin A produced by thymocytes regulates the migration of murine bone marrow cells. *Cell. Immunol.* 249:46–53. doi:10.1016/j.cellimm.2007.11.002

Kim, H., W.J. Kim, S.T. Jeon, E.M. Koh, H.S. Cha, K.S. Ahn, and W.H. Lee. 2005. Cyclophilin A may contribute to the inflammatory processes in rheumatoid arthritis through induction of matrix degrading enzymes and inflammatory cytokines from macrophages. *Clin. Immunol.* 116:217–224. doi:10.1016/j.clim.2005.05.004

Knowles, J.W., R.L. Reddick, J.C. Jennette, E.G. Shesely, O. Smithies, and N. Maeda. 2000. Enhanced atherosclerosis and kidney dysfunction in eNOS(−/−)Apoe(−/−) mice are ameliorated by enalapril treatment. *J. Clin. Invest.* 105:451–458. doi:10.1172/JCI8376

Kockx, M., W. Jessup, and L. Kritharides. 2010. Cyclosporin A and atherosclerosis—cellular pathways in atherogenesis. *Pharmacol. Ther.* 128:106–118. doi:10.1016/j.pharmthera.2010.06.001

Kuhlencordt, P.J., R. Gyurko, F. Han, M. Scherrer-Crosbie, T.H. Aretz, R. Hajjar, M.H. Picard, and P.L. Huang. 2001. Accelerated atherosclerosis, aortic aneurysm formation, and ischemic heart disease in apolipoprotein E/endothelial nitric oxide synthase double-knockout mice. *Circulation.* 104:448–454. doi:10.1161/hc2901.091399

Li, H., and U. Förstermann. 2009. Prevention of atherosclerosis by interference with the vascular nitric oxide system. *Curr. Pharm. Des.* 15:3133–3145. doi:10.2174/138161209789058002

Liao, D.F., Z.G. Jin, A.S. Baas, G. Daum, S.P. Gygi, R. Aebersold, and B.C. Berk. 2000. Purification and identification of secreted oxidative stress-induced factors from vascular smooth muscle cells. *J. Biol. Chem.* 275:189–196. doi:10.1074/jbc.275.1.189

López-Miranda, J., E. Vilella, F. Pérez-Jiménez, A. Espino, J.A. Jiménez-Perepérez, L. Masana, and P.R. Turner. 1993. Low-density lipoprotein metabolism in rats treated with cyclosporine. *Metabolism.* 42:678–683. doi:10.1016/0026-0495(93)90232-D

Lungu, A.O., Z.G. Jin, H. Yamawaki, T. Tanimoto, C. Wong, and B.C. Berk. 2004. Cyclosporin A inhibits flow-mediated activation of endothelial nitric-oxide synthase by altering cholesterol content in caveolae. *J. Biol. Chem.* 279:48794–48800. doi:10.1074/jbc.M313897200

Nakashima, Y., A.S. Plump, E.W. Raines, J.L. Breslow, and R. Ross. 1994. ApoE-deficient mice develop lesions of all phases of atherosclerosis throughout the arterial tree. *Arterioscler. Thromb.* 14:133–140.

Nakashima, Y., E.W. Raines, A.S. Plump, J.L. Breslow, and R. Ross. 1998. Upregulation of VCAM-1 and ICAM-1 at atherosclerosis-prone sites on the endothelium in the ApoE-deficient mouse. *Arterioscler. Thromb. Vasc. Biol.* 18:842–851.

Oemar, B.S., M.R. Tschudi, N. Godoy, V. Brovkovich, T. Malinski, and T.F. Lüscher. 1998. Reduced endothelial nitric oxide synthase expression and production in human atherosclerosis. *Circulation.* 97:2494–2498.

Ojo, A.O. 2006. Cardiovascular complications after renal transplantation and their prevention. *Transplantation.* 82:603–611. doi:10.1097/01.tp.0000235527.81917.fe

Pan, H., C. Luo, R. Li, A. Qiao, L. Zhang, M. Mines, A.M. Nyanda, J. Zhang, and G.H. Fan. 2008. Cyclophilin A is required for CXCR4-mediated nuclear export of heterogeneous nuclear ribonucleoprotein A2, activation and nuclear translocation of ERK1/2, and chemotactic cell migration. *J. Biol. Chem.* 283:623–637. doi:10.1074/jbc.M704934200

Parmar, K.M., H.B. Larman, G. Dai, Y. Zhang, E.T. Wang, S.N. Moorthy, J.R. Kratz, Z. Lin, M.K. Jain, M.A. Gimbrone Jr., and G. García-Cardeña. 2006. Integration of flow-dependent endothelial phenotypes by Kruppel-like factor 2. *J. Clin. Invest.* 116:49–58. doi:10.1172/JCI24787

Podrez, E.A., D. Schmitt, H.F. Hoff, and S.L. Hazen. 1999. Myeloperoxidase-generated reactive nitrogen species convert LDL into an atherogenic form in vitro. *J. Clin. Invest.* 103:1547–1560. doi:10.1172/JCI5549

Satoh, K., Y. Kagaya, M. Nakano, Y. Ito, J. Ohta, H. Tada, A. Karibe, N. Minegishi, N. Suzuki, M. Yamamoto, et al. 2006. Important role of endogenous erythropoietin system in recruitment of endothelial progenitor cells in hypoxia-induced pulmonary hypertension in mice. *Circulation.* 113:1442–1450. doi:10.1161/CIRCULATIONAHA.105.583732

Satoh, K., T. Matoba, J. Suzuki, M.R. O'Dell, P. Nigro, Z. Cui, A. Mohan, S. Pan, L. Li, Z.G. Jin, et al. 2008. Cyclophilin A mediates vascular remodeling by promoting inflammation and vascular smooth muscle cell proliferation. *Circulation.* 117:3088–3098. doi:10.1161/CIRCULATIONAHA.107.756106

Satoh, K., P. Nigro, T. Matoba, M.R. O'Dell, Z. Cui, X. Shi, A. Mohan, C. Yan, J. Abe, K.A. Illig, and B.C. Berk. 2009. Cyclophilin A enhances vascular oxidative stress and the development of angiotensin II-induced aortic aneurysms. *Nat. Med.* 15:649–656. doi:10.1038/nm.1958

Seizer, P., T. Schönberger, M. Schött, M.R. Lang, H.F. Langer, B. Bigalke, B.F. Krämer, O. Borst, K. Daub, O. Heidenreich, et al. 2010. EMMPRIN and its ligand cyclophilin A regulate MT1-MMP, MMP-9 and M-CSF during foam cell formation. *Atherosclerosis.* 209:51–57. doi:10.1016/j.atherosclerosis.2009.08.029

Sherry, B., N. Yarlett, A. Strupp, and A. Cerami. 1992. Identification of cyclophilin as a proinflammatory secretory product of lipopolysaccharide-activated macrophages. *Proc. Natl. Acad. Sci. USA.* 89:3511–3515. doi:10.1073/pnas.89.8.3511

Suzuki, J., Z.G. Jin, D.F. Meoli, T. Matoba, and B.C. Berk. 2006. Cyclophilin A is secreted by a vesicular pathway in vascular smooth muscle cells. *Circ. Res.* 98:811–817. doi:10.1161/01.RES.0000216405.85080.a6

Tangirala, R.K., E.M. Rubin, and W. Palinski. 1995. Quantitation of atherosclerosis in murine models: correlation between lesions in the aortic origin and in the entire aorta, and differences in the extent of lesions between sexes in LDL receptor-deficient and apolipoprotein E-deficient mice. *J. Lipid Res.* 36:2320–2328.

Tegeder, I., A. Schumacher, S. John, H. Geiger, G. Geisslinger, H. Bang, and K. Brune. 1997. Elevated serum cyclophilin levels in patients with severe sepsis. *J. Clin. Immunol.* 17:380–386. doi:10.1023/A:1027364207544

Uittenbogaard, A., Y. Ying, and E.J. Smart. 1998. Characterization of a cytosolic heat-shock protein-caveolin chaperone complex. Involvement in cholesterol trafficking. *J. Biol. Chem.* 273:6525–6532. doi:10.1074/jbc.273.11.6525

Vaziri, N.D., K. Liang, and H. Azad. 2000. Effect of cyclosporine on HMG-CoA reductase, cholesterol 7alpha-hydroxylase, LDL receptor, HDL receptor, VLDL receptor, and lipoprotein lipase expressions. *J. Pharmacol. Exp. Ther.* 294:778–783.

Weber, C., A. Zernecke, and P. Libby. 2008. The multifaceted contributions of leukocyte subsets to atherosclerosis: lessons from mouse models. *Nat. Rev. Immunol.* 8:802–815. doi:10.1038/nri2415

Weintraub, N.L. 2009. Understanding abdominal aortic aneurysm. *N. Engl. J. Med.* 361:1114–1116. doi:10.1056/NEJMcibr0905244

Won, D., S.N. Zhu, M. Chen, A.M. Teichert, J.E. Fish, C.C. Matouk, M. Bonert, M. Ojha, P.A. Marsden, and M.I. Cybulsky. 2007. Relative reduction of endothelial nitric-oxide synthase expression and transcription in atherosclerosis-prone regions of the mouse aorta and in an in vitro model of disturbed flow. *Am. J. Pathol.* 171:1691–1704. doi:10.2353/ajpath.2007.060860

Xu, Q., M.C. Leiva, S.A. Fischkoff, R.E. Handschumacher, and C.R. Lyttle. 1992. Leukocyte chemotactic activity of cyclophilin. *J. Biol. Chem.* 267:11968–11971.

Yurchenko, V., G. Zybarth, M. O'Connor, W.W. Dai, G. Franchin, T. Hao, H. Guo, H.C. Hung, B. Toole, P. Gallay, et al. 2002. Active site residues of cyclophilin A are crucial for its signaling activity via CD147. *J. Biol. Chem.* 277:22959–22965. doi:10.1074/jbc.M201593200

Zhu, C., X. Wang, J. Deinum, Z. Huang, J. Gao, N. Modjtahedi, M.R. Neagu, M. Nilsson, P.S. Eriksson, H. Hagberg, et al. 2007. Cyclophilin A participates in the nuclear translocation of apoptosis-inducing factor in neurons after cerebral hypoxia-ischemia. *J. Exp. Med.* 204:1741–1748. doi:10.1084/jem.20070193